Partial Discharge Diagnosis on GIS Based on Envelope Detection

LI LI-XUE, HUANG CHENG-JUN, ZENG YI, JIANG XIU-CHEN
Dept. of Electrical Engineering
Shanghai Jiao Tong University
Room 237, telecommunications group Building, 800#, Dongchuan Road, Shanghai, China
Email address: lilixue@sjtu.edu.cn xcjiang@sjtu.edu.cn

Abstract: In order to detect and identify the defects on GIS, the ultra-high frequency envelope detection circuit and high-speed data acquisition system was designed, and the tests of five typical defects for GIS were made in the laboratory and the envelope signal was acquired based on Ultra-high frequency (UHF) envelop detection circuit. And wavelet denoising technique was used to reduce the white noise of the measurement envelop signal. A large number of experiments show that time-domain characteristics of partial discharge signals generated by the same defect model are about the same, envelopes are nearly identical too. The time-domain characteristics of partial discharge signals generated by different defect models are different, and their envelope shapes are different too. A new method of pattern recognition was proposed which analyses the characteristic parameters of the envelope signal at time-domain with BP neural network. A large number of test data in Lab indicate that the method is effective.

Key-Words: GIS, partial discharge, pattern recognition, UHF, envelop detection, BP neural network

1 Introduction

Detection of partial discharge is presently the most effective method for GIS insulation detection and diagnosis [1]. Partial discharge serves as both a warning of and a representation of the degraded insulation of the GIS, and partial discharge may cause further degradation of the insulation [2][3]. Earlier insulation defects inside the GIS can be discovered effectively through partial discharge detection so as to avoid further failure and improve the reliability of the GIS.

The UHF method [4], which is widely used for the online detection on GIS, receives high-frequency electromagnetic waves generated by the partial discharge of the GIS through UHF sensors. There are several data processing methods for failure identification, these include: Phase Resolved Partial Discharge (PRPD)[5-6], frequency-spectrum analysis [7-8], time domain waveform analysis [9] etc.

A novel method based on UHF is introduced which uses a UHF envelope detection circuit to extract the envelope signal of the UHF signal. And a high-speed data collecting system was adopted for sampling. The partial discharge defects can be classified by extracting the fingerprints of the time domain waveforms of the envelope signals and the BP neural network.

Compared with the real-time sampling method using a wideband oscilloscope, this method greatly reduces sampling velocity, data size and computational cost, thus improving the efficiency of the defect diagnosis system. Frequency-spectrum analysis method must use a spectrum analyzer so that it's difficult for on-line monitoring. This method is especially useful for high voltage DC system where PRPD method can't be used for the absence of the information of phase.

2 Design of Hardware System

The hardware of the partial discharge detection system for GIS at UHF based on envelope detection is composed of: a built-in UHF sensor, wideband amplifier, bandpass filter, GSM wave trap circuit,

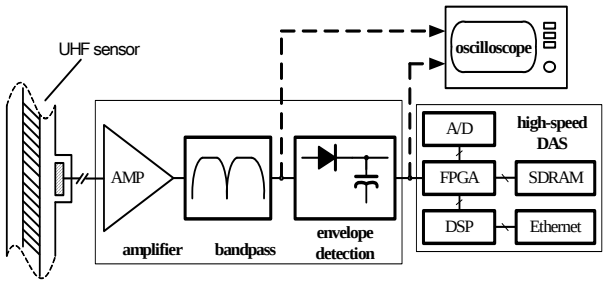

Fig. 1 Partial discharge diagnostic system for GIS at UHF based on envelope detection circuit

envelope extract circuit and high-speed data collection circuit etc., as shown in Fig. 1. The partial discharge signals received by the UHF sensor are from –80dBm to –15dBm. They are amplified by a low noise, wideband amplifier whose gain is programmable. The maximum gain that can be achieved is 50dB. The filter circuit comprises the bandpass filter and the GSM trap of 900MHz. The frequency of the bandpass filter is determined by the disturbance on testing site, and general disturbing signals on site include electric corona, FM broadcasting station, GSM signals, wireless LAN signals etc. In this study, a 300–1500MHz filter and GSM trap of 900MHz were used to reduce most of the wireless disturbance as the main energy of the UHF signal was in the range 300–1500MHz. The envelope detection circuit is composed of RF diodes and high-frequency capacitors, etc. (see Fig. 1).

Envelop circuit is one of the key parts of this method for PD detection. The charging time for the envelope detection circuit needs to be less than l nano-second (ns) so as to reduce the peak-value error. Due to their actual natural parameter limits, diode components have the equivalent on-resistance [10] at room temperature by the equation (1) below.

$$R_j \approx \frac{0.026}{I_s + I_b} \qquad (1)$$

Where I_s is the (reverse) saturation current of the diode, and I_b is the current flowing through the diode. If the bias current applied to the diode is 10μA, its equivalent resistance is about 2.6kΩ, then the equivalent integral time constant is 2.6ns; therefore, when the input of the detection circuit is the GIS partial discharge UHF signals in non-continuous oscillating sine waves, there is a certain peak-value detection error. It has been shown experimentally, that the error was no more than 10%. Thus it can meet the engineering requirements.

The collection velocity adopted in this study is 250M samples per second (SPS). The measurement error caused by sampling frequency can be calculated by the equation in (2).

$$\delta = (1 - e^{-1/(fRC)}) \times 100\% \qquad (2)$$

Where f is the sampling frequency of a data acquisition system; R and C are the discharging resistance and capacitance, respectively; the discharging resistance R is 470kΩ; and the capacitance is 1pF. The peak-value sampling error δ is then about 1% which meets the measurement requirement.

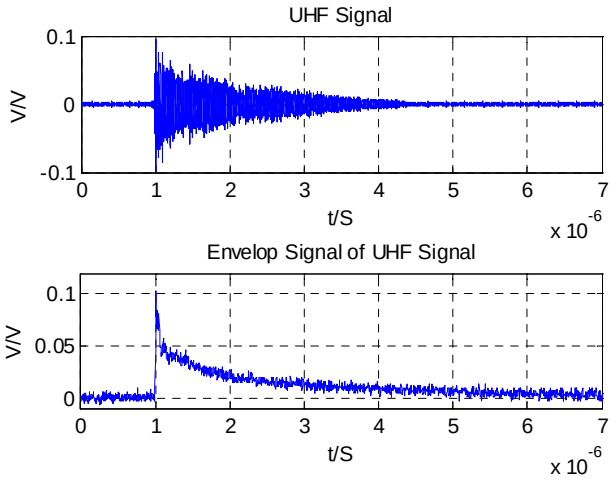

Fig. 2 UHF signal and its envelope signal of the defect model of needle on conductor

The high-speed data acquisition system is composed of: high-speed A/D, FPGA, DDRII SDRAM, DSP etc., where the high-speed A/D, FPGA and SDRAM form a sampling unit, and data are stored from A/D to SDRAM by using a method similar to direct memory access (DMA) and controlled by FPGA; the DSP communicates through an Ethernet interface and triggers sampling processes and carries out pre-treatments such as filtering etc.

3 Denoising with wavelet

3.1 Noise characteristic of UHF envelop signal

External interferences may directly affect the sensitivity and reliability of the PD signal analysis, and reduce the credibility of PD measurement. The major external interference sources include [11-14]:

(i) Discrete spectral interferences (DSI), which are from radio transmissions and communication systems.

(ii) Repetitive and stochastic pulse shaped interferences, which are from power electronics, switching operations, lighting and so on.

(iii) White noises, which are from electromagnetic of the space, amplifier and other hardware circuits.

In this study, an envelop circuit is used to extract the envelop of the PD signal received by UHF sensor. At the process of envelop detection, DSI noises are transferred into DC, and repetitive and stochastic pulse shaped interferences are nearly like the PD signal at the shape but can be removed by pattern recognition for the different characteristic parameters. So white noises are the major noises which influence the extract of the characteristic parameters and the sensitivity and reliability of the PD detection.

3.2 DWT denoising technique

The wavelet transform of a function *f(x)* at the scale S and position x is given by the convolution product [15][16], where parameter S is sampled along the dyadic sequence (2^j) j Z

$$W_{2^j} f(x) = f * \psi_{2^j}(x) = \frac{1}{2^j}\int_{-\infty}^{+\infty} f(t)\psi(\frac{x-t}{2^j})dt \quad (3)$$

The function *f(x)* can be reconstructed from its wavelet transform, and the reconstruction is stable, if and only if there exists two constants A 0 and B 0 such that

$$A \le \sum_{j=-\infty}^{+\infty} \left|\hat{\psi}(2^j\omega)\right|^2 \le B \quad (4)$$

One can then prove that there exists a (non-unique) reconstructing wavelet $\hat{X}(x)$ whose Fourier transform satisfies

$$\sum_{-\infty}^{+\infty} \hat{\psi}(2^j\omega)\hat{X}(2^j\omega) = 1 \quad (5)$$

The function *f(x)* is recovered from its dyadic wavelet transform with the equation (6).

$$f(x) = \sum_{-\infty}^{+\infty} W_{2^j} f * X_{2^j}(x) \quad (6)$$

According to the application results of wavelet theory, the module maximum value of the wavelet coefficient for white noise is decreased with the decomposition level increasing, whereas the MMV of the wavelet coefficient for the PD signal increases with the decomposition level increase [16]. In this paper, Daubechie-2(db2) wavelet was used as mother wavelet.

Removal interferences and noises from signal is one of the applications of DWT technique. DWT can decompose the original polluted signal in different frequency resolution according to multi-resolution analysis (MRA) method. The MRA of DWT is equivalent to filtering a time domain original signal by means of a pair of filters, i.e., the decomposition high pass filter(DHF) and the decomposition low pass filter(DLF). The DHF and DLF are called quadrature mirror filters (QMF). When decomposition, the original signal passes through the DHF and DLF with down-sampling algorithm by two to produce the high frequency components (also named high frequency coefficients) and the low

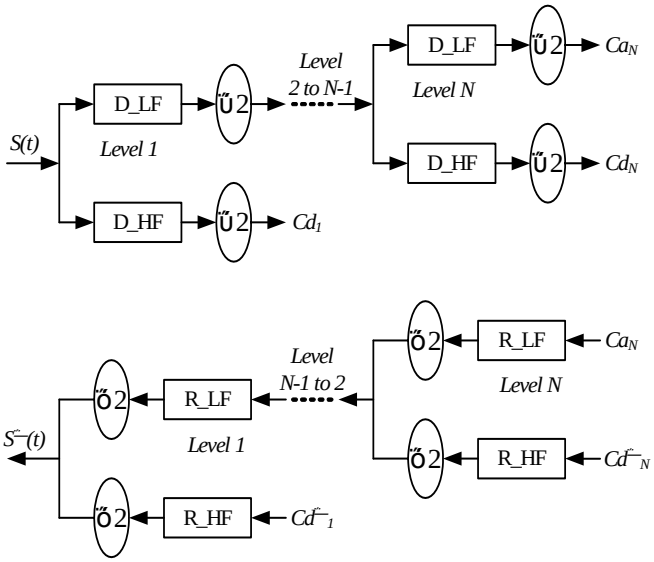

Fig.3 Signal decomposition and reconstruction

frequency coefficients (also named low frequency coefficients), i.e., the details and approximations. The low frequency components are decomposed further at a degree that frequency resolution is satisfying. The structure of MRA is shown in figure 3. Where N is the final decomposition scale; Ca_i is the low frequency coefficient at scale i; and Cd_i is the high frequency coefficient at scale i. The down-sampling by two expresses that every sampling reduced the sampling rate by half. That is to say that signal length and frequency are halved at every time when the signal passes through the QMF.

Generally, after decomposition, some of the coefficients have a main energy relating to the signal and others are relating to the interferences and noises. From this view of point, if we remove or reduce the energies relating to the interferences and noises in specific frequency resolution, the signal will be completely reconstructed and extracted. In practice, it is difficult to separate completely the signal energy and noises energy from the DWT coefficients. General researches for removal or suppression of noises are to set a threshold for the coefficient in a scale, i.e., most of the noise energies can not pass through the threshold but the signal can. DWT denoising methods can be carried out either by hard threshold process or by soft threshold process.

The reconstruction of signal is the reverse process of the decomposition. It is realized by the reverse discrete wavelet transform (IDWT). The low frequency coefficient and modified high frequency coefficient at every scale pass through the reconstruction low pass filter (RLF) and the reconstruction high pass filter (RHF) respectively with up-sampling by two to assemble the low frequency coefficient of the up scale. Eventually, the signal is extracted.

From above discussion, the denoising process of signal by DWT technique includes three steps below.

Step1: Signal decomposition. Select a suitable wavelet, and determine a decomposing scale. And then, decompose the original noised signal to the final scale. Daubechie-2(db2) wavelet is used as mother wavelet and scale N is 6 in this paper.

Step2: Threshold selection and quantitative change. Choose a threshold for every high frequency coefficient from the scale 1 to the scale N and make a soft threshold or a hard threshold quantitative change. A scale-dependent automatic threshold is used by the algorithm as shown in equation (7).

$$\lambda_j = \frac{m_j}{0.6745}\sqrt{2 \cdot \log n_j} \qquad (7)$$

Where λ_j is threshold value of approximation coefficients or detail coefficients at scale j, m_j is the median value of corresponding coefficients at scale j and n_j is the signal length at scale. Rescaling factor 0.6745 is used to limit the coefficients fluctuation during denoising. It is well suitable for zero mean white noises suppression [18][19].

Step3: Signal reconstruction. Use the decomposed low frequency coefficient of the scale N and the high frequency coefficients from scale 1 to scale which has been quantitative changed to reconstruct the signal.

3.3 Simulation

According to determination methods discussed above, simulation studies have been done. Simulated PD

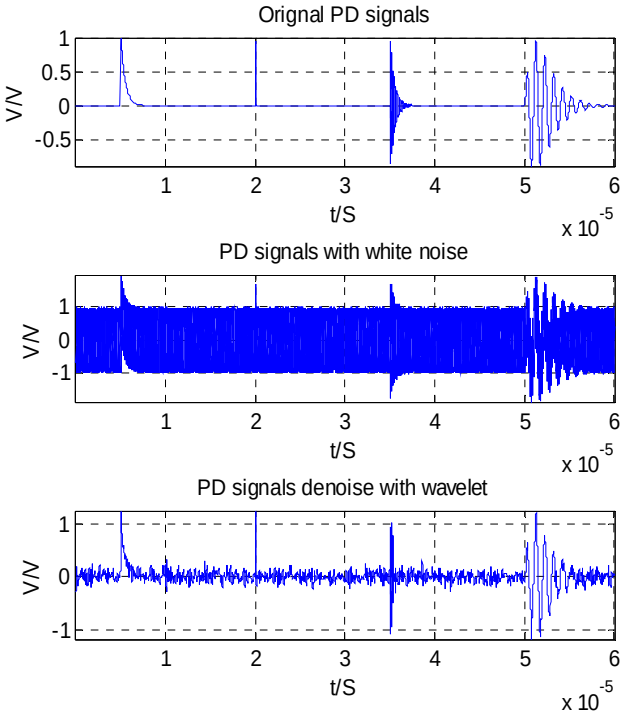

Fig.4 Simulation of extracting PD signal from noises

signals based on mathematic model [20], PD signal with white noises and PD signal denoised with wavelet are shown in figure. 4 respectively. Where the sampling rate is 250MHz and the sampling time is 60μs.

3.4 PD envelop signal denoised with wavelet

A practical envelop signal composed with noise has been denoised by the wavelet. As a result, white noise was reduced obviously and the signal to noise ratio (SNR) was increased (see figure. 5).

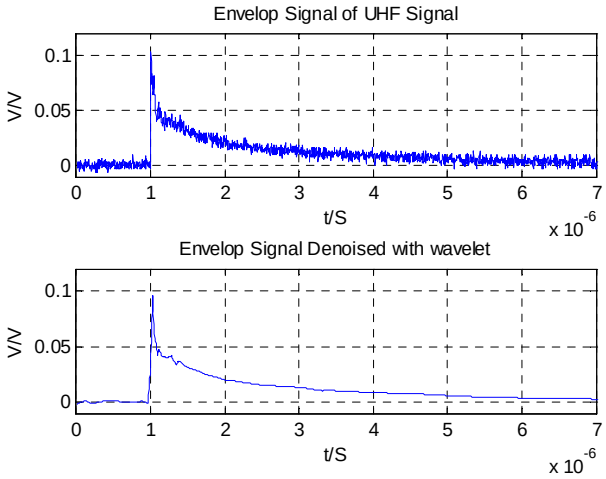

Fig.5 Practical envelop signal denoised by the wavelet

4 Testing of Defect Models

4.1 Test system

GIS partial discharge test system comprises: high-voltage power supply without partial discharge, GIS tank, GIS defect models, traditional partial discharge detecting instrument, UHF measurement system, wide-band oscilloscope, etc. The connecting diagram is shown in fig. 6.

The defect model test was carried out on a 220kV GIS test system operated by a GIS manufacturer (as shown in Fig. 3). The main equipment comprised: 550kV fully sealed transformer booster, partial discharge test instrument, GIS cavity about 20m long, multifunctional meter, partial discharge diagnostic system based on envelope detection circuit, Agilent DSO54853A wideband oscilloscope etc. The background partial discharge of the system was about 1.1pC.

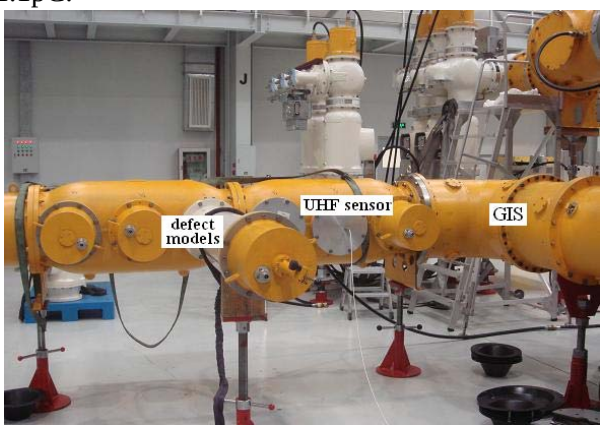

Fig.7 220kV GIS Test System

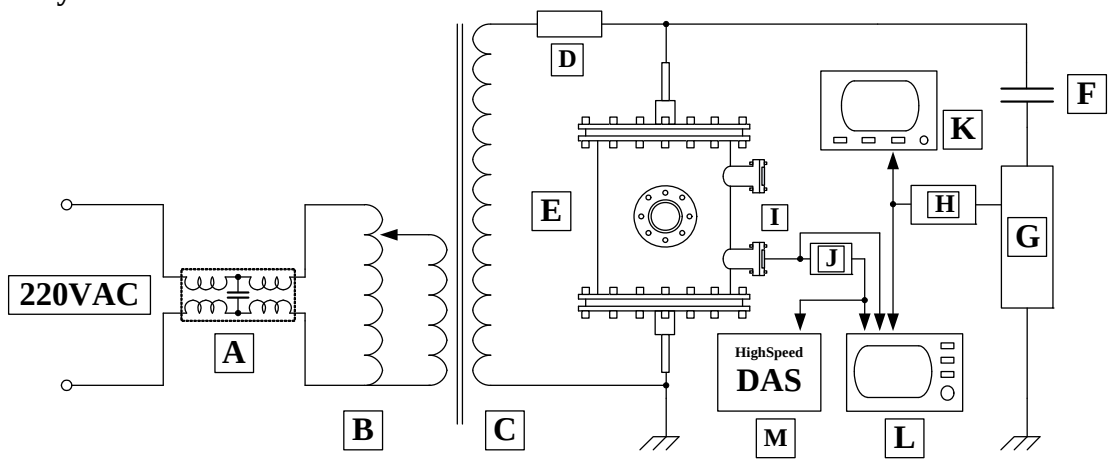

A EMI Filter; B voltage regulator; C transformer booster;
D protective resistor; E GIS entity; F coupled capacitor;
G measured impedance; H amplifier using pulse current method;
I UHF sensor; J UHF amplifier;
K traditional partial discharge detecting instrument;
L Agilent DSO54853A wide-band oscilloscope;
M high-speed data collecting system

Fig.6 Connecting diagram of UHF method test using envelope detection

4.2 Defect models

The defects which may cause partial discharge in GIS include: free metallic particles which can travel in the GIS cavity, bad contact of conductive parts, inner gaps formed during insulator manufacture, surface marks caused by test flashover and the rough surface of the electrode, or metallic particles on the insulator etc.[21-22], as shown in Fig. 8.

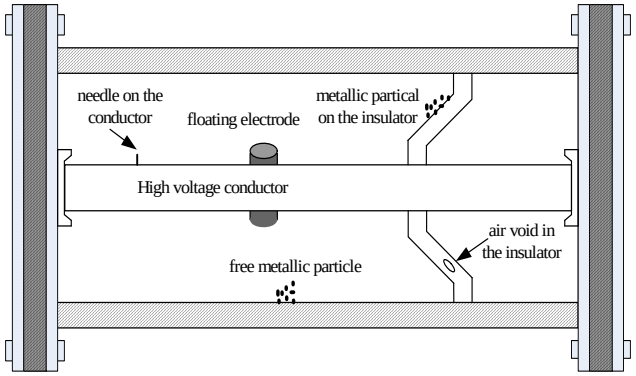

Fig.8 Diagram of several insulation defects in GIS

According to the analysis above, five defect models were designed: a free metallic particle model, a needle on conductor model, an air void in the insulator model, a metallic particle on the insulator model and a floating electrode model. Metallic particles may be produced during manufacture, assembly and running, which can accumulate charge and can travel under the impact of AC electric fields. They travel and discharge in a random manner. Discharge is most likely to occur when they are closer to high-voltage conductors, but without being in contact. A sharp burr may appear on the surface of high-voltage conductors due to bad fabrication, or damage and friction during installation. An electric flashover may not occur in the standard power-frequency state, however, discharge may occur if there is a rapid, impacting, transient excess voltage. Both inner gaps formed during manufacture of the insulator and a difference in the contraction coefficients of the epoxy resin and metal electrode can lead to the formation of inner air-bubbles and gaps in the insulators. The discharge caused by bad contact between the conductive parts, especially the floating parts, is fairly high, and tends to repeat. It is probable that these insulation defect models of the GIS may cause partial discharge phenomenon in the GIS, partial discharge in insulators may even erode the insulating material and then develop into electric branches, eventually resulting in a puncture of the insulation.

4.3 Data analysis

The five defect models were installed separately in the GIS and it was filled with SF_6 gas under 0.61MPa pressure, and then kept stable for about 10 minutes. Voltage was added step by step and envelope signals of UHF signal obtained. Typical envelope signals of free metallic particle model and needle on conductor model are shown in figure 9(a) to 9(e).

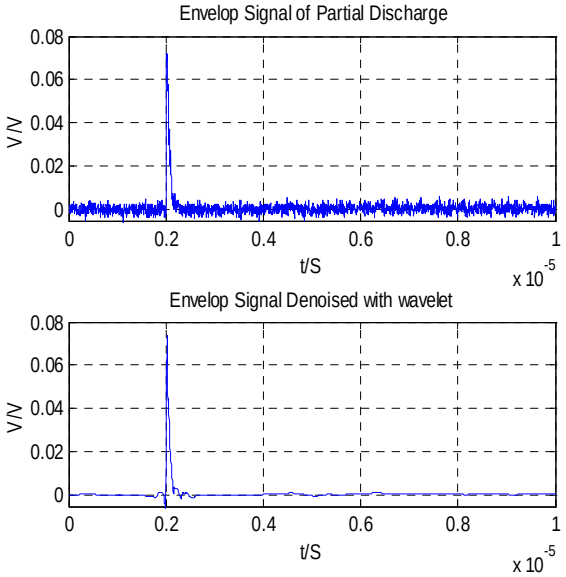

Fig.9(a) PD envelop of free metallic particle

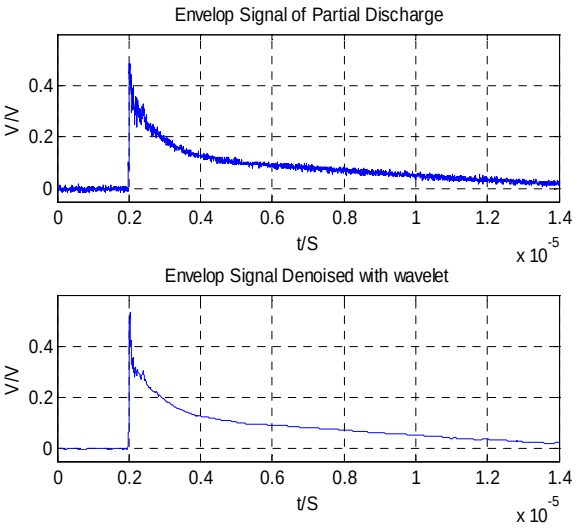

Fig.9(b) PD envelop of needle on conductor

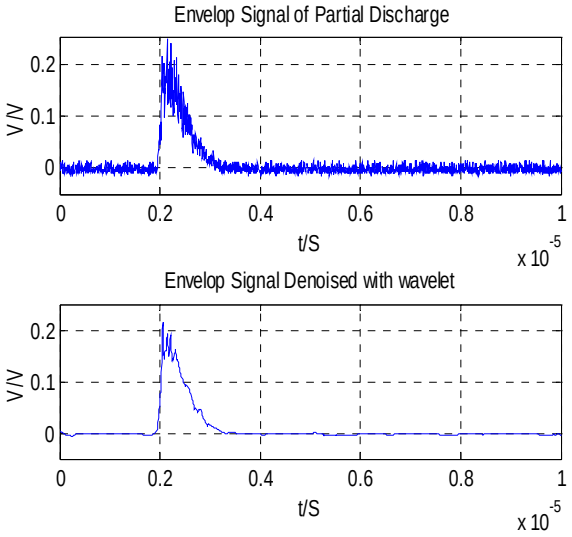

Fig.9(c) PD envelop of air void in the insulator

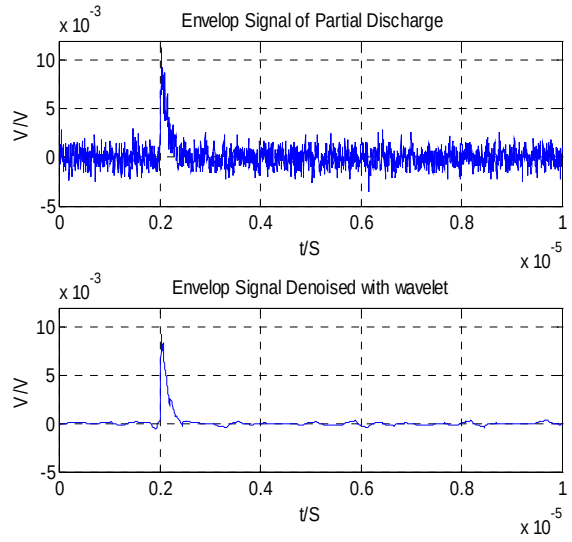

Fig.9(d) PD envelop of floating electrode

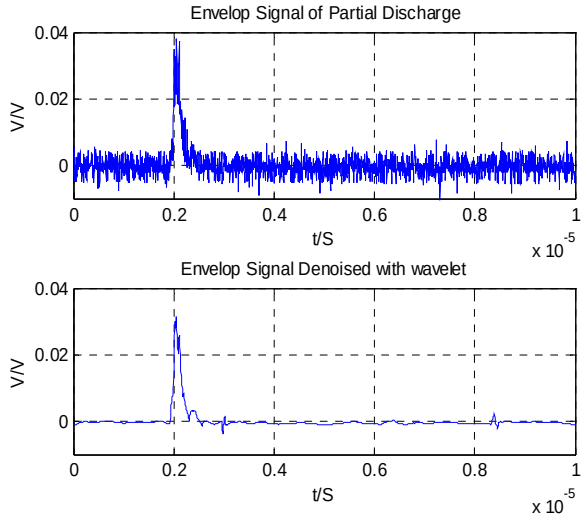

Fig.9(e) PD envelop of metallic particle on the surface of insulator

From the above test results we can see that characteristics of envelope signals generated by different defect models differ somewhat, wherein, discharge signals generated by air-void in insulator model has the characteristics of dual-exponential dying oscillation while all signals in other defect models have the characteristics of single-exponential dying oscillation. As for the discharge amplitude, needle on high-voltage conductor has the highest discharge amplitude, air-void in insulator is the next, free metallic particle and metallic particle on insulator surface have comparable discharge amplitude, and discharge signals of floating electrode are the lowest. The pulse width of needle on high-voltage conductor is also the highest, insulator inner air-void is next, and discharge signals generated by free metallic particles last for the shortest time.

5 Classification of defects

A large number of experiments showed that the time-domain characteristics of the partial discharge signals and the envelopes generated by the same defect model are about the same. Both the time-domain characteristics of the partial discharge signals and the envelope shapes generated by the different defect models are different. Therefore, the characteristic parameters of the envelope signals can be sampled, and these parameters can be used with neural-network algorithms for pattern recognition.

5.1 Characteristic parameters

Envelope shapes of partial discharge signals can be represented through time-domain characteristic parameters [22] which include: wave head time t_h, pulse rising-edge time t_r, pulse falling-edge time t_d, pulse width of discharge $t_{50\%}$, apparent discharge endurance time $t_{10\%}$, skewness s_k and kurtosis k_u.

$$K_u = \frac{E(x_i - \mu)^4}{\sigma^4} \qquad (8)$$

$$S_k = \frac{E(x_i - \mu)^3}{\sigma^3} \qquad (9)$$

Table 2 Characteristic parameters of five defects

Defect type / Parameters	Free metallic particles	Needle on conductor	Air void in insulator	Metallic partial on insulator	Floating electrode
t (μs)	0.028	0.044	0.140	0.044	0.024
t_r (μs)	0.024	0.024	0.136	0.020	0.020
t_d (μs)	0.108	7.624	0.600	0.232	0.144
$t_{50\%}$ (μs)	0.064	0.220	0.128	0.096	0.048
$t_{10\%}$ (μs)	0.136	7.668	0.740	0.256	0.168
S_k	10.2299	1.872	3.726	5.980	2.620
K_u	116.917	7.931	17.254	49.025	18.537

Where x_i is the number i of sampling points, μ is the average value of $\{x\}$, σ is the standard deviation of $\{x\}$, and E is the expectation of $\{x\}$.

Kurtosis K_u describes the degree of probability distribution of extraneous variable being centralized at an average value, namely the variety kurtosis of distribution function. The larger K_u is, the more intensive one discharge pulse in single-discharge waveform grows. Skewness S_k describes the symmetry properties of probability distribution of extraneous variable. S_k is the symmetry degree of one distribution relative to the corresponding parameter average-value of one single-discharge waveform. If $S_k > 0$, the distribution function average-value is in positive asymmetry; if $S_k = 0$, the distribution function average-value is in full symmetry; if $S_k < 0$, the distribution function average-value is in negative asymmetry.

By using those characteristic parameters mentioned above, the shape of time-domain waveform can be described. Discharge signals generated by different defect models have corresponding different characteristic parameters. Therefore, model recognition of different discharge models can be carried out.

Those seven characteristic parameters were used to describe the shape of the envelope which is characteristic of the UHF signal. Table 2 shows the typical characteristic parameters of five defect models.

5.2 Classification using BP neural network

Model recognition is a method in which recognition and classification of objects are carried out according to some characteristics. The neural-network model recognition method simulates the thinking process of the human brain, so it has very high intelligence. The BP network, which adopts a back-propagation training algorithm, namely the BP algorithm, is a multilayer feed-forward neural network with very wide applications. BP network algorithm is used for pattern recognition in this paper based on data analysis of different defects and the fingerprints of the envelope signals [24].

5.3 Classification results

The BP network adjusts the relevant weight of neurons according to the mean square error between the actual and desired output in the training process. When the maximum of the absolute value of the error between the actual output and the desired output is smaller than the specified error, δ, the training ends. The smaller the obtained value of δ, the longer the training time lasts. Table 3 shows that the recognition hit rate can be improved by reducing δ, though the corresponding training time will increase. When δ is smaller than a specified value, its influence on the recognition results will be unimportant. Thus,

defining δ as 0.001 is adequate for the recognition hit rate.

Table 3 Hit rates (%) of BP network recognition under different error conditions

Training error δ / Defect models	0.005	0.002	0.001
Free metallic particle	85	93	97
Needle on conductor	100	100	100
Air void in insulator	96	95	97
Metallic partial on insulator	86	90	96
Floating electrode	97	100	100

6 CONCLUSIONS

1) A partial discharge diagnostic system for GIS at UHF based on an envelope detection circuit was designed and experiments on five defect models were carried out.

2) A method of time-domain analysis for envelope signals of GIS partial discharge was proposed. By sampling the characteristic parameters of envelope signals and using model recognition based on a BP neural network, defect types could be distinguished with a very high recognition rate.

3) Pattern recognition can be achieved without the information of the phase which used in PRPD. This may be very useful in DC applications.

Reference:

[1] T.Sakakibara, T. Nakajima, S. Maruyama, et al. Development of GIS fault location system using pressure wave sensors. IEEE Trans. on Power Delivery, Vol.14, No. 2, 1999, pp. 371-377

[2] Y.Hasegawa, K.Izumi, A.Kobayshi, et al. Investigation on phenomena caused by insulation abnormalities in actual GIS. IEEE Trans. on Power Delivery, Vol.9, No.2, 1994, pp. 796-804

[3] E.A.Feilat, S.Grzybowski, et al. Breakdown and aging behavior of composite insulation system under DC and AC high voltages. WSEAS Transactions on Circuits and Systems, Vol.4, No.7, 2005, pp. 780-787

[4] J.S.Pearson, B.F.Hampton, A.G.Sellars. A continuous UHF monitor for gas-insulated Substations. IEEE Transactions on Electrical Insulation, Vol.26, No.3, 1991, pp. 469-478

[5] B.F.Hampton, J.S.Pearson, C.J.Jones, T.Irwin, I.M.Welch, B.M.Pryor. Experience and Progress with UHF diagnostics in GIS. CIGRE, 1992, 15/23-03

[6] N.Achatz, J.Gorablenkow, U.Schichler, B.Hampton, J.Pearson. Features and benefits of UHF partial discharge monitoring systems for GIS [C]. Proceedings of 2005 International Symposium on Electrical Insulating Materials, Japan, 2005. Electrical Insulating Materials, (ISEIM 2005), 2005, pp. 722-725

[7] Toshihiro Hoshino, Katsumi Kato, Naoki Hayakawa. Frequency Characteristics of Electromagnetic Wave Radiated From GIS Apertures. IEEE Transactions on Power Delivery, Vol.16, No.4, 2001, pp. 552-557

[8] M.Doi, H.Muto, H.Fujii, M.Kamei, Frequency spectrum of various partial discharges in GIS, Proceedings of 1998 International Symposium on Electrical Insulating Materials, Japan, 1998, pp. 441-444

[9] Zhou Qian, Tang Ju, Tang Ming, Xie Yan-bin, Liu Ming-jun. Mathematical Model of Four Typical Defects for UHF Partial Discharge in GIS. Proceedings of the CSEE, Vol.26, No.8, 2006, pp. 99-105

[10] Technical Data of HSMS-282x datasheet, www.agilent.com/semiconductors.

[11] L.Satish and B.Nazneen. Wavelet-based Denoising of Partial Discharge Signals Buried in Excessive Noise and Interference. IEEE Trans. Dielectr. Electr. Insul., Vol.10, 2003, pp. 354-367.

[12] Zhou-Sheng Zhang and Deng-Ming Xiao. Noise-based Wavelet Denoising Technique for Partial Discharge Measurement. WSEAS Transactions on Circuits and Systems, Vol.7, 2008, pp. 535-546

[13] Yan Xiao, Yu Wei-yong, et al. Suppression of partial discharge's discrete spectral interference based on spectrum estimation and wavelet packet transform. WSEAS Transactions on Circuits and Systems, Vol.4, No.11, 2005, pp. 1508-1515

[14] Qian Yong, Huang Cheng-Jun, et al. Investigation of multi-wavelet denoising in partial discharge detection. WSEAS Transactions on Circuits and Systems, Vol.5, No.1, 2006, pp. 85-91

[15] Z.M.Li, Y.P.Feng, J.Q.Chen, X.G.Zheng. Wavelet Analysis Used in UHF Partial Discharge Detection in GIS. IEEE International Conference on Power System Technology, Vol.1, 1998, pp. 163-166

[16] Heric, Dusan, et al. Reconstruction of object contours using directional wavelet transform. WSEAS Transactions on Computers, Vol 4, No 10, 2005, pp 1305-1312

[17] S.Mallet, H.Wang, et al. Singularity detection and processing with wavelet. IEEE Trans. Inform. Theory, Vol 2, 1992, pp. 617-643

[18] X.Ma, C.Zhou and I.J.Kemp. Interpretation of wavelet analysis and its application in partial discharge detection, IEEE Trans. Diel. Elect.Insul., Vol.9, 2002, pp. 446-457.

[19] H.Zhang, T.R.Blackburn, B.T.Phung and D.Sen. A novel wavelet transform technique for on-line partial discharge measurements part 2: on-site noise rejection application, IEEE transactions on dielectrics and electrical insulation, Vol.14, No. 1, 2007, pp. 15-22.

[20] Huang Cheng-jun, Yu Wei-yong. Study of adaptive filter algorithm based on wavelet analysis in suppressing PD's periodic narrow bandwidth noise. Proceedings of the CSEE. Vol.23, No.1, 2003, pp. 107-111

[21] Feroz Ahmed, Ahmad Bin Darus, Zulkalnain Yusoff, Md.Enamul Haque. Defect detection and identification of sources in GIS based on labortatory and on-site experience. Conference Record of the 1998 IEEE International Symposium on Electrical Insulation, USA, 1998, pp. 73-76

[22] Tang Ju, Zhou Qian, Xu Zhong-rong et al. Establishment of mathematical model for partial discharge in GIS using UHF method. Proceedings of the CSEE, Vol.25, No.19, 2005, pp. 106-110

[23] Chen Xiao-lin, Jiang Yan et al. Fingerprint Analyzing Method of Ultra-wideband Partial Discharge Time-domain Waveform. High Voltage Engineering, 2001, Vol.27, No.4, 2001, pp. 13-15

[24] M.G.Danlikas, N.Gao, M.Aro. Partial discharge recognition using neural networks: a review. Electrical Engineering. Vol.85, No.2, 2003, pp. 87-93